Research paper

Upper water mass variability in the Anegada–Jungfern Passage, NE Caribbean, during the last 11,100 cal. yr

The Holocene
2017, Vol. 27(9) 1291–1307

DOI: 10.1177/0959683616687378
journals.sagepub.com/home/hol
SAGE

Andrea Fischel,[1] Marit-Solveig Seidenkrantz,[2] Dirk Nürnberg,[3] Michal Kucera[4] and Antoon Kuijpers[5]

Abstract

Using qualitative and quantitative analyses of planktonic foraminifera assemblages, $\delta^{18}O$ measurements, Mg/Ca–temperature relationship (*Globigerinoides ruber* pink sensu stricto) data and sea-surface temperatures (SSTs) derived from artificial neural network (ANN) transfer functions, a reconstruction was made of upper water mass variability in the Anegada–Jungfern Passage (AJP), northeastern Caribbean Sea, over the last *c.* 11,100 years. Our record is based on the study of two marine sediment cores and reveals three main circulation stages during the Holocene. In the early-Holocene (11,100–6300 cal. yr BP), ANN-based SST estimations indicate moderately cooler than present winter condition in the NE Caribbean with SSTs of ~25.5°C. These conditions presumably reflect advection of well-mixed upper water masses from the Guyana upwelling area associated with a strong Atlantic Meridional Overturning Circulation (AMOC) and enhanced trade wind activity, linked to a more northerly location of the inter-tropical convergence zone (ITCZ). Between 6300 and 3700 cal. yr BP, a relative warming of winter SSTs (~26.5°C) was probably related to a weaker circulation and upper water mass mixing because of less intense trade wind activity, as the ITCZ moved southwards. From 3700 cal. yr BP to the present, the region was characterised by small seasonal SST variations and generally stable winter and summer SSTs. The data suggest a minor shift in the (sub)surface inflow pattern during the last 2000 years, possibly related to changes in Northern Hemisphere large-scale atmospheric circulation also observed at higher latitude. The ANN-based temperature pattern is supported by fluctuations in the Mg/Ca-derived temperature record, although temperature maxima derived from the Mg/Ca ratio appear anomalously high. On a Holocene timescale, we conclude that the northeastern Caribbean SST and circulation regime have been mainly dependent on the position of the ITCZ, which, in turn, is controlled by changes in hemispheric solar insolation.

Keywords

Caribbean palaeoceanography, Holocene, inter-tropical convergence zone, planktonic foraminifera, sea-surface temperature, tropical Atlantic

Received 21 December 2015; revised manuscript accepted 5 December 2016

Introduction

The Caribbean Sea forms an important gateway for the Atlantic Meridional Overturning Circulation (AMOC), as this region represents the transit area for low-latitude Atlantic surface and subsurface water masses and more distant southern-source waters on their way into the Gulf Stream–North Atlantic Current system. Water masses from the central Atlantic Ocean enter the northeastern Caribbean Sea via a number of deep, narrow passages between the islands; the Anegada–Jungfern Passage (AJP) being the most significant of these gateways (Jury, 2011; Stalcup and Metcalf, 1973; Wüst, 1964). The Caribbean Current entrains the inflowing water masses westwards, where they pass through the Strait of Yucatan and enter the Gulf of Mexico (Figure 1). Here, they form the Loop Current that merges with the Antilles Current, thereby creating the Florida Current–Gulf Stream system of the North Atlantic which forms the western branch of the North Atlantic Subtropical Gyre (Figure 1; Gordon, 1967; Kameo et al., 2004; Wüst, 1964).

In the Caribbean Basins and the Gulf of Mexico, the low latitudinal intense insolation and a high evaporation rate further contribute to the warmth and salinity of the already relatively warm surface waters advected from the central Atlantic. This leads to the warmth of the Florida Current and the Gulf Stream. Thus, the Caribbean region, including the AJP, plays a crucial role for meridional water mass exchange and transport of heat and salt from the tropics to the northern North Atlantic (Fratantoni et al., 1997; Johns et al., 2002).

The northern Caribbean climate today is warm and humid, with a mean annual air temperature of 27°C and an annual

[1]NIRAS A/S, Denmark
[2]Centre for Past Climate Studies, Department of Geoscience, Aarhus University, Denmark
[3]GEOMAR Helmholtz Centre for Ocean Research Kiel, Germany
[4]MARUM - Center for Marine Environmental Sciences, University of Bremen, Germany
[5]Geological Survey of Denmark and Greenland, Denmark

Corresponding authors:
Andrea Fischel, NIRAS A/S, Ceres Alle 3, DK-8000 Aarhus C, Denmark.
Email: anf@niras.dk

Marit-Solveig Seidenkrantz, Centre for Past Climate Studies, Department of Geoscience, Aarhus University, Høegh-Guldbergs Gade 2, DK-8000 Aarhus C, Denmark.
Email: mss@geo.au.dk

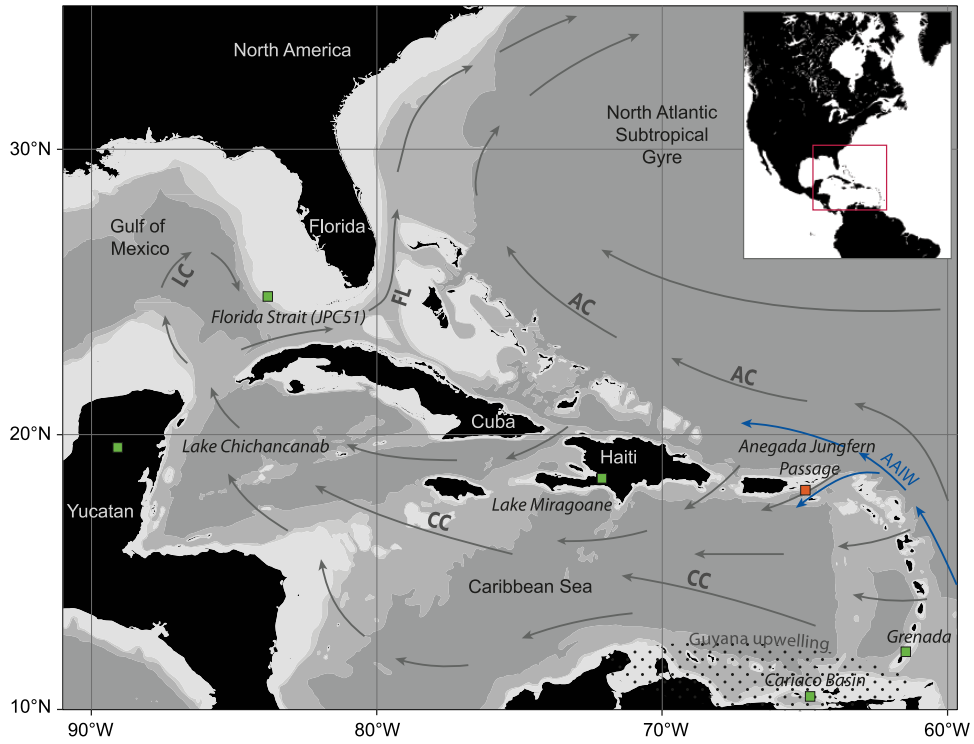

Figure 1. Map of the southwestern North Atlantic showing the present-day bathymetry and surface ocean circulation (grey arrows). The location of the study region, the Anegada–Jungfern Passage in the NE Caribbean, is marked by a red rectangle (core sites north of St Croix: gravity core Ga307-Win-12GC from 3960 m water depth and box core Ga307-Win-02BC from 1026 m water depth). Green rectangles: other climate records, mentioned in the text: Lake Miragoane, Haiti (from Hodell et al., 1991), Florida Strait (Schmidt et al., 2012), Lake Chichancanab (Hodell et al., 1995), Grenada (Fritz et al., 2011) and Cariaco Basin (Haug et al., 2001).
AC: Antilles Current; CC: Caribbean Current; FC: Florida Current; LC: Loop Current.

precipitation of about 1100 mm (Gamble and Curtis, 2008). Sea-surface temperatures (SST) at 10 m water depth range between 26.1°C and 28.3°C with a mean annual of 27.4°C (World Ocean Atlas, 1998). The Caribbean region is every year affected by tropical storms and hurricanes originating from the wider tropical Atlantic region (Inoue et al., 2002). Caribbean climate is directly controlled by the position of the inter-tropical convergence zone (ITCZ), where converging NE and SE trade winds creates a low-pressure convection zone with high precipitation rates (Philader et al., 1996; Schmidt et al., 2006). With variations of about ±2° latitude, the modern ITCZ has an average position at approximately 5°N, with a furthest northerly approach in boreal summer at 12°N (Arbuszewski et al., 2013). In addition to the seasonal variations in the position of the ITCZ, the long-term N–S migration of the ITCZ is largely determined by decadal to millennial changes in solar forcing (Haug et al., 2001; Schneider et al., 2014). In the early-Holocene, orbital precession led to increased Northern Hemisphere insolation and warming and correspondingly northward migration of the ITCZ. At shorter centennial to decadal time scales, ITCZ variations can be linked to relative warming of the Northern or Southern Hemisphere, with preferred migration into latitudes of the warmer hemisphere (Arbuszewski et al., 2013). Variations in the tropical SST and the location of the ITCZ have also been linked to climate variability at mid- and high latitudes, most pronounced on millennial to glacial/interglacial timescale (e.g. Haug et al., 2001; Lea et al., 2003; Schneider et al., 2014; Ziegler et al., 2008). Previous studies by Knudsen et al. (2011) showed that variations in ITCZ position can also be correlated to changes in North Atlantic SST pattern and precipitation on multi-decadal time scales. In terms of SST variations, this implies further N–S migration of the ITCZ away from the colder hemisphere (Arbuszewski et al., 2013).

Caribbean climate is further affected by far-field effects of more distant ocean–atmosphere interaction phenomena, the El Niño–Southern Oscillation (ENSO; Giannini et al., 2000; Jury et al., 2007; Malmgren et al., 1998; Taylor et al., 2002) and the North Atlantic Oscillation (NAO; Giannini et al., 2001; Marshall et al., 2001; Rogers, 1984), centred in the tropical Pacific and North Atlantic regions, respectively. Warmer-than-average temperatures and reduced tropical storm frequency occur during El Niño years, and colder-than-average temperatures prevail during La Niña years (Giannini et al., 2000; National Weather Service San Juan, PR Weather Forecast Office, 2010). During El Niño years, the Caribbean also experiences higher-than-average precipitation rates in the dry season (December–April) and low precipitation rates in the wet season (May–November), while the opposite pattern is seen during La Niña years (Giannini et al., 2000; National Weather Service San Juan, PR Weather Forecast Office, 2010).

The NAO has a weaker, primarily seasonally dependent influence on Caribbean climate (Giannini et al., 2001; Jury et al., 2007; Marshall et al., 2001; Rogers, 1984). During years with a positive winter NAO index, strong westerlies and SW–NE-oriented moisture transport in the North Atlantic lead to lower-than-average annual precipitation in the Caribbean, while Caribbean SST is slightly reduced (Malmgren et al., 1998).

Despite the significance of the region for the AMOC and for the general climate of the central and North Atlantic region, long-term studies of northeastern Caribbean ocean circulation and Holocene climate are limited. This especially applies to the AJP, a major conduit for water mass transport into the Caribbean. This study will present a record of Holocene surface and subsurface water mass variability and SST variations in the northeastern Caribbean based on several analytical techniques applied to the planktonic foraminifera fauna preserved in two marine sediment cores. The main purpose is to investigate possible links of changes in tropical (sub)surface water flow in the AJP with ocean and climate signals from the wider North Atlantic region.

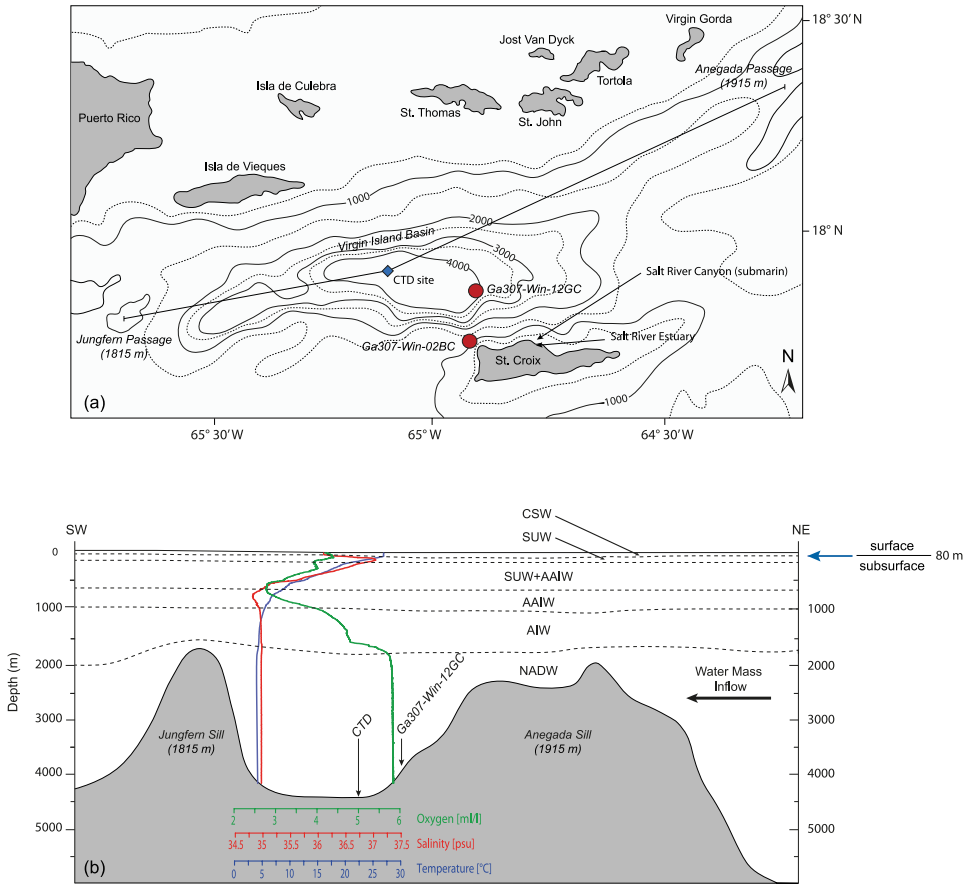

Figure 2. (a) Map showing the core sites for Ga307-Win-12GC and GA307-Win-02BC (red circles) and the location of the CTD profile (blue diamond) in the Anegada–Jungfern Passage. The bathymetry is based on a seismic and multibeam survey carried out during the Galathea3 Expedition Leg 16. The black line illustrates the location of the transect shown in Figure 2b. SRE: Salt River Estuary on St Croix; the Salt River Canyon (SRC) extend from the mouth of the estuary to the insular slope, where core Ga307-WIN12GC is located. (b): Transect between the Anegada Sill and the Jungfern Sill, including the CTD profile from the deepest part of the Virgin Island Basin obtained March 2007. Temperature (blue), salinity (red) and oxygen (green) are illustrated as a top–bottom profile. Based on the CTD, the hydrography in the Virgin Island Basin could be differentiated into five distinctive water mass layers – 0–100 m: Caribbean surface water (CSW), 100–200 m: subtropical underwater (SUW), 200–700 m: mixed layer of SUW and Antarctic Intermediate Water (AAIW), 700–1000 m: AAIW, 1000–1900 m: Atlantic Intermediate Water (AIW) and 1900–4200 m: North Atlantic Deep Water (NADW). The blue arrow points to the lower boundary of the late winter (March) thermocline zone at *c.* 80 m water depth. The approximate comparable location of core site Ga307-Win-12GC is shown. The distance to core site GA307-Win-02BC is too large to allow marking its location on this transect.

Hydrographic setting and modern planktonic foraminiferal distribution of the AJP

The Caribbean basins are ventilated by water masses from the Atlantic entering the Caribbean via several deep passages. The AJP is considered to be one of the primary gateways for this inflow of Atlantic water to the eastern Caribbean Sea (Dietrich, 1963; Stalcup et al., 1975). This ENE–WSW-oriented channel conduit displays two topographic features: the Anegada Sill in the northeast and the Jungfern Sill at its southwestern end (Figure 2a). The water mass inflow from the Atlantic Ocean into the Caribbean basins is limited by the Anegada Sill (Figure 2b). A sill depth of 1915 m allows an inflow of (upper) North Atlantic Deep Water (NADW) from the western Atlantic into the Virgin Islands Basin (Fratantoni et al., 1997). Similarly, the Jungfern Sill (Figure 2b), at a depth of 1815 m between the Virgin Islands Basin and the deep Venezuelan Basin towards the southwest (Stalcup et al., 1975), also controls the water mass exchange, especially of the NADW and the Antarctic Intermediate Water (AAIW).

The water mass transport through the passage is characterised by a distinct stratification (Wüst, 1964). This is also illustrated by a 4162-m-deep CTD (conductivity–temperature–depth) profile (Figure 2), obtained in March 2007 from the deepest part of the Virgin Island Basin (17°57.79N, 65°00.58W) during Leg 16 of the Danish Galathea3 Expedition around the world (Kuijpers and Project Group, 2007). Five distinct water mass strata could be recognised in the AJP: the upper 50 m consists of Caribbean surface water (CSW), which shows a maximum water temperature of 26.8°C, which is within the range recorded in the World Ocean Atlas (i.e. 26.1–28.3°C with an annual average of SST = 27.4°C; Levitus et al., 1994; World Ocean Atlas, 1998). The CSW mass represents the local mixed layer, whose lower boundary is known as the seasonal thermocline. In the northeastern Caribbean Sea, maximum depth of the thermocline is found close to 100 m in January–March and a minimum of near 25 m in the fall (Jury, 2011). In Figure 2, the late winter (March) thermocline is indicated by an arrow pointing to a decrease in temperature at about 80 m water depth. Underneath the CSW, the high-saline (37‰) subtropical underwater (SUW) is found at 50–180 m below sea surface (see Figure 2b). The SUW is formed by surface evaporation in the subtropical Atlantic and mainly originates from the Sargasso Sea and the southern and central parts of the North Atlantic Subtropical Gyre, from where it spreads widely throughout the tropical Atlantic and Caribbean Basins (Hernandez-Guerra and Joyce, 2000; Metcalf, 1976; O'Connor et al., 2005). The nutrient-rich, low-saline AAIW mass is found at 500–1000 m water depth, with its core at 700–1000 m depth (Kameo et al.,

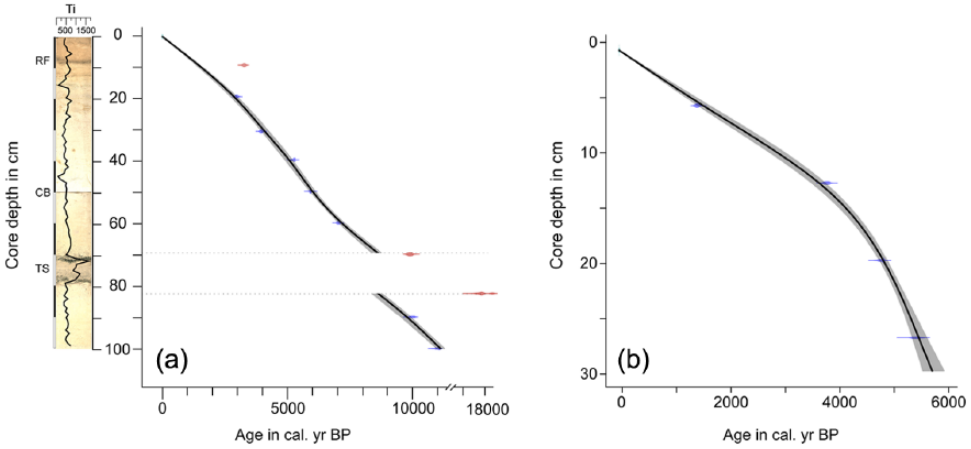

Figure 3. (a) The age model of the upper 100 cm of the gravity core Ga307-Win-12GC and (b) the 26-cm-long box core Ga307-Win-02BC are based on 7 and 4 radiocarbon dates, respectively. In addition, three outliers were identified in Ga307-Win-12GC. The material used for dating consists of *Globigerinoides ruber* (white), and the ^{14}C datings were calibrated using the Marine09 ^{14}C dataset (Reimer et al., 2009) with a reservoir correction of 400 years. The age–depth model was established with the open-source software R and the 'clam' package (Blaauw, 2010). The best model was calculated after running 10,000 iterations using a smooth spline fit. The age model includes best-fit (black line), two-sigma probability (grey area) and radiocarbon dates (blue). Samples marked in red: three radiocarbon measurements identified as outliers. A: in addition to the age model of Ga307-Win-12GC, the sedimentology and Titanium (Ti) content in counts per second is shown. The modern redox front (RF) is located at 9 cm core depth. The core break (CB) is seen in 50 cm core depth. Furthermore, a turbidite sequence (TS) of at least two turbidite strata could be identified in the core interval 69–82 cm.

2004; Wüst, 1964). The water mass between 200 and 500 m is characterised by decreasing temperatures and salinity and is interpreted as a mixed layer originating from the SUW and AAIW (Kameo et al., 2004; Worthington, 1959).

The present planktonic foraminiferal fauna of the warm surface waters of the northeastern Caribbean Sea are characterised by tropical and subtropical taxa. The upper 20 m is characterised by high proportions of *Neogloboquadrina dutertrei* and *Globigerinita glutinata*, often associated with cyclonic eddies (Schmuker and Schiebel, 2002). However, in the Anegada Passage, where Sargasso Sea water flows into the Caribbean Sea, lower standing stocks of these species indicate more oligotrophic conditions. The SUW masses entering the Caribbean Sea through the Anegada Passage are characterised by higher concentrations of *Globorotalia truncatulinoides* relative to the adjacent water masses. For further information on the link between upper water mass hydrography and modern planktonic faunal distribution in the adjacent eastern Caribbean and tropical Atlantic, refer to Steph et al. (2009).

Materials and methods

Sediment cores

Gravity core Ga307-Win-12GC (17°50.80N, 64°48.7290W; 3960 m water depth) and box core Ga307-Win-02BC (17°45.1805N, 64°58.2614W; 1026 m water depth) were obtained in March 2007 during the Danish Galathea3 Expedition, Leg 16, on board HMS '*Vædderen*' (Kuijpers and Project Group, 2007). The CTD profile (Figure 2b) was collected at 17°57.79N, 65°00.58W, close to core Ga307-Win-12GC (March 2007). The core sites are located in the north of the island of St. Croix, U.S. Virgin Islands (Figure 2a). Gravity core Ga307-Win-12GC covers the upper 510 cm sediment of a submarine fan, located at the foot of the insular slope, in close proximity of the Salt River Bay and downslope of the Salt River Canyon (Figure 2a; Kuijpers and Project Group, 2007). Box core Ga307-Win-02BC recovered 26 cm of sediment from the upper part of the insular slope. In this study, the results of the Holocene part of the cores (the upper 100 cm of gravity core Ga307-Win-12GC and the entire box core Ga307-Win-02BC) are presented. Box core Ga307-Win-02BC was included in this study as it provides an oceanographic record for the past 5000 years, but with a higher resolution than obtained for gravity core Ga307-Win-12GC, which covers the entire Holocene (see below).

Lithology

The sediments of the cores consist of light beige to grey, fine-grained, mainly calcareous ooze, clay and silt. In core Ga307-Win-12GC, three layers of greenish-purple to dark-grey sand are observed (core depth: 8–9, 69–71 and 76–79 cm; Figure 3a). The initially dark, purple layer at 8–9 cm core depth has been interpreted as the manganese horizon of the redox front and is thus not related to sediment deposition; it faded because of oxygenation after opening the core. However, a thin sandy layer just below (9–10 cm; Figure 3a) and the two layers within the interval 69–79 cm consist of coarse-grained sand with a fining upward trend and are considered to represent turbidite sequences (TS; Figure 3a). The two lower turbidites could also be recognised as a prominent peak in magnetic susceptibility and in the x-ray fluorescence core scanning (XRF) trace element data as maxima in Titanium (Ti; Figure 3a) and Iron (Fe; not shown) in the otherwise predominantly calcareous (Ca) sediment. Box core Ga307-Win-02BC consists of fine-grained light-grey to light-beige calcareous ooze throughout.

Age models

The chronologies of the sediment cores are based on accelerated mass spectrometry radiocarbon (AMS ^{14}C) dating conducted on monospecific samples of *G. ruber* (white) in the >100 µm fraction (Table 1). The AMS ^{14}C datings were carried out at the Aarhus AMS Centre, Department of Physics and Astronomy, Aarhus University, Denmark. All dates were calibrated using the Marine09 ^{14}C calibration dataset (Reimer et al., 2009) with a standard reservoir correction of 400 years (average $\Delta R = 28$; standard deviation (*SD*) = 36 for the area; Reimer and Reimer, 2001). Being aware that reservoir ages may vary spatially and temporally, we choose the 400-year estimate to stay consistent to published proxy records. The respective age–depth models were constructed using the open-source software R and the 'clam' package (Blaauw, 2010). The best model for both cores was calculated after running 10,000 iterations using a smooth spline fit.

Table 1. Radiocarbon dates based on monospecific samples of tests of the planktonic foraminiferal species *Globigerinoides ruber* (white). Samples marked with (*) are from the intervals identified as a turbidite layer and are not included in the age model. All dates were calibrated using the Marine09 ^{14}C dataset (Reimer et al., 2009) with a reservoir correction of 400 years. The age–depth models were made using the open-source software R and the 'clam' package (Blaauw, 2010). The modelled age for the cores is calculated as the best approximation after running 10,000 iterations using a smooth spline fit.

Core depth in cm	Lab code	Material	^{14}C age ± 1σ	$\delta^{13}C$ ± 1σ	Calibrated age range 2σ (95% probability) in cal. yr BP	Modelled age in cal. yr BP
Ga307-Win-02BC						
5–6	AAR 15251	*G. ruber*	1845 ± 24	0.72 ± 0.05	1393–1605	1487
12–13	AAR 15252	*G. ruber*	3814 ± 23	1.12 ± 0.05	3481–3733	3619
19–20	AAR 15253	*G. ruber*	4554 ± 26	1.03 ± 0.05	4730–4870	4799
26–27	AAR 12420	*G. ruber*	5055 ± 55	1.71 ± 0.05	5333–5598	5450
Ga307-Win-12GC						
9–10▲	AAR 15393	*G. ruber*	3363 ± 30	0.16 ± 0.05	3137–3330	3296
19–20	AAR 15394	*G. ruber*	3152 ± 26	0.66 ± 0.05	2845–3039	2820
30–31	AAR 15395	*G. ruber*	3936 ± 25	0.91 ± 0.05	3827–4016	4062
39–40	AAR 15396	*G. ruber*	4897 ± 30	0.62 ± 0.05	5107–5302	5036
49–50	AAR 15397	*G. ruber*	5523 ± 40	1.17 ± 0.05	5776–6003	5983
59–60	AAR 15398	*G. ruber*	6520 ± 34	1.12 ± 0.05	6935–7143	7156
69–70*	AAR 12248	*G. ruber*	8613 ± 47	0.76 ± 0.05	9573–9956	–
81–82*	AAR 15399	*G. ruber*	15,172 ± 60	0.76 ± 0.05	17,661–18,089	–
89–90	AAR 15400	*G. ruber*	9182 ± 40	0.67 ± 0.05	9839–10,145	9707
99–100	AAR 15401	*G. ruber*	10,024 ± 40	0.96 ± 0.05	10,879–11,149	11,129

The age model for the upper 100 cm of gravity core Ga307-Win-12GC is based on seven AMS ^{14}C measurements, with three outliers identified at 9, 70 and 81 cm core depth (Table 2, Figure 3a). The outliers at 9, 70 and 81 cm core depth correspond to the intervals associated with the turbidite layers (Figure 2a). These intervals are not included in further discussions and are excluded from the age model of the core. In total, 13 cm of turbidite deposits were thus omitted from the sediment record. The resulting age model shows sedimentation rates (for the non-turbidite sediments) ranging between 6 and 9 cm in 1000 years and a temporal resolution of most data in this study of 400–600 years.

Four AMS ^{14}C dates have been used to establish the age model for the 26-cm-long box core Ga307-Win-02BC (Table 2, Figure 3b). The sedimentation rates in this core vary between 3 and 5 cm per 1000 year, that is, a data resolution of 150–300 years. The highest sedimentation rate is observed at 22–26 cm core depth (5000–5400 cal. yr BP).

XRF core scanning

XRF using the AVAATECH system (both 10 and 30 keV) was applied at 1-cm resolution to core Ga307-Win-12GC at the Royal Netherlands Institute for Sea Research (NIOZ) in Texel, the Netherlands. The Titanium data are shown in Figure 3 as counts per second (cps).

Stable isotopes

Stable isotope measurements for this core, conducted on monospecific samples of *G. ruber* (pink) from the size fraction 200–400 μm, were performed at the Woods Hole Oceanographic Institution in Massachusetts, US, using a Finning MAT252 mass spectrometer with an SD of the isotope values in accordance to the National Bureau Standards (NBS) carbonate standards NBS-19.

Planktonic foraminiferal assemblages and artificial neural network analyses

The subsamples for foraminiferal analyses each represent a 1-cm core slice. The wet samples were weighed and wet-sieved at 1000, 100 and 63 μm; subsequently, each fraction was dried. The dry 100–1000 μm fraction was subsequently dry-sieved at 150 μm as the 150–1000 μm fraction to allow comparison with database on modern benthic foraminiferal distribution (Kucera et al., 2005).

Qualitative and quantitative planktonic foraminiferal analyses of the 0.150–1.0 mm fraction were applied to both cores: the planktonic foraminiferal assemblages were analysed at a 5-cm resolution in gravity core Ga307-Win-12GC and at 1-cm resolution in box core Ga307-Win-02BC. The fraction >1000 μm mainly consists of mollusc and shell fragments, echinoid spines and a very small number of large benthic foraminifera. Thus, this fraction was not included in the quantitative analyses of planktonic foraminifera in this study. All samples were split using a micro-splitter up to seven times to obtain a representative aliquot with a minimum of 300 specimens of planktonic foraminifera. The statistical error in foraminiferal assemblage counts depends on the number of specimens counted, but a count of 300 specimens is sufficient for detailed interpretations and species making out at least 3% of an assemblage is considered to be statistically reliable (Fatela and Taborda, 2002), while values <1% may cease to be meaningful (Buzas, 1990), although the data are still useful as part of the general context. The taxonomy of planktonic foraminifera is based on the studies by Bé (1977) and Hemleben et al. (1989) (Table 2).

In order to track the inflow and structure of the upper (thermocline) water masses, a qualitative approach has been established, separating the assemblages into a shallow dwelling fauna, characterising the surface water condition (CSW) and a subsurface dwelling fauna, addressing the water masses below 100 m (including SUW and the late winter thermocline zone; Figures 4 and 5). The shallow-water community is defined by the most common surface dwellers *G. ruber* (both pink and white varieties; Bé, 1967; Bé et al., 1971; Boltovskoy et al., 2000; Hemleben et al., 1989), *Globigerinoides sacculifer* with/without sac (w/o sac; Hemleben et al., 1989; Mulitza et al., 1997), *Globigerinoides conglobatus* (Hemleben et al., 1989) and *Globoturborotalita rubescens* (Bé, 1967; Mulitza et al., 1997). These taxa are all described to reach a maximum in relative abundance within the upper 100 m water depth in the tropical Atlantic (Bé and Tolderlund, 1971). The subsurface group encompasses species that reach their highest relative abundance in water depth below 100 m (mainly 100–200 m), which implies the lower boundary of the

Table 2. List of planktonic foraminiferal taxa identified in the material. Species marked with (*) are used as key species to define the surface water mass, and species marked with (**) are grouped to characterise the subsurface water stratum in this study.

Taxa	Author and year of description
Candeina nitida	d' Orbigny (1839)
Globigerina bulloides	d' Orbigny (1826)
Globigerina falconensis	Blow (1959)
Globigerinella calida	Parker (1962)
Globigerinella digitata	Brady (1879)
Globigerinella siphonifera	d' Orbigny (1839)
Globigerinita glutinata	Egger (1895)
Globigerinita minuta	Natland (1938)
Globigerinita uvula	Ehrenberg (1862)
*Globigerinoides conglobatus**	Brady (1879)
*Globigerinoides ruber**	d' Orbigny (1839)
*Globigerinoides sacculifer**	Brady (1877)
*Globorotalia crassaformis***	Galloway (1927)
Globorotalia hirsuta	d' Orbigny (1839)
*Globorotalia inflata***	d' Orbigny (1839)
Globorotalia menardi	d' Orbigny (1865)
Globorotalia scitula	Brady (1882)
Globorotalia theyeri	Fleischer (1974)
*Globorotalia truncatulinoides***	d' Orbigny (1839)
*Globorotalia tumida***	Brady (1977)
Globorotalia ungulata	Bermudez (1960)
*Globoturborotalita rubescens**	Hofker (1956)
Globoturborotalita tenella	Parker (1958)
Hastigerina digitata	Rhumbler (1911)
Hastigerina pelagica	d' Orbigny (1839)
Neogloboquadrina dutertrei	d' Orbigny (1839)
Neogloboquadrina incompta	Cifelli (1961)
Neogloboquadrina pachyderma	Ehrenberg (1862)
Orbulina universa	d' Orbigny (1839)
Pulleniatina obliquiloculata	Parker and Jones (1865)
Sphaeroidinella dehiscens	Parker and Jones (1865)
Tenuitella iota	Parker (1962)
Turborotalita quinqueloba	Natland (1938)

winter thermocline zone and underlying SUW. The group includes the species *Globorotalia tumida* (Bé and Tolderlund, 1971; Hemleben et al., 1989), *Globorotalia crassaformis* (Bé and Tolderlund, 1971; Jones, 1967), *Globorotalia inflata* (Bé, 1959; Bé and Tolderlund, 1971; Hemleben et al., 1989) and *G. truncatulinoides* (Bé, 1959; Bé et al., 1971; Hemleben et al., 1989; Mulitza et al., 1997). The deep-dwelling species *Globorotalia scitula* has not been included in the subsurface group as it lives even deeper in the water column below the thermocline (Birch et al., 2013). Species with variable or unknown depth requirements are not grouped (see Table 2). The cumulative species abundances of the surface dwellers and subsurface community have been used as an index of surface and subsurface/thermocline water mass properties.

A Q-mode cluster analysis was carried out in order to determine the main faunal trends and to define biofacies (zones A, B and C) and their boundaries. The cluster analysis was carried out in depth-constrained mode, using the PAST software (Hammer et al., 2001). It was performed on both cores separately, comprising a data set of 18 samples for the core Ga307-Win-12GC (Figure 4) and 28 samples for the core Ga307-Win-02BC (not shown), applying an unweighted paired group method, which generates clusters from similarity matrices, calculated using the Euclidean similarity coefficient.

Winter and summer SSTs were reconstructed for both cores using the artificial neural network (ANN) transfer function technique (Malmgren et al., 2001) based on the planktonic foraminifera assemblage counts and including all species, both surface and deeper dwellers as is standard for this technique (Malmgren et al., 2001). The SST estimation is based on the MARGO North Atlantic dataset, which is calibrated to seasonal SST at the 10-m level in the water column (Kucera et al., 2005). According to this definition, the reconstructed SSTs thus represent temperatures at 10 m water depth. The SST reconstructions based on the ANN transfer function technique are averages of the outputs of 10 networks trained on different partitions of the calibration data set (Kucera et al., 2005). Winter STT has an average SD from the networks of 0.24, while the average SD of the summer SST is 0.40. The root mean square error of prediction for the MARGO North Atlantic dataset is approximately 1°C (Kucera et al., 2005). The ANN method has been tested in the Caribbean on high-resolution records off Puerto Rico, where the ANN reconstructions were shown to follow closely instrumental records, especially for the winter season (Malmgren et al., 2001; Nyberg et al., 2002).

Mg/Ca ratios

Additional palaeo-thermometer information has been acquired using the Mg/Ca ratio of the surface dweller species *G. ruber* (pink) sensu stricto. For this purpose, monospecific samples including 20 specimen from the size fraction 0.315–0.355 mm at 5 cm spacing were collected and processed in the laboratories of the GEOMAR Helmholtz Centre for Ocean Research Kiel, Germany. The sample cleaning procedure for Mg/Ca measurements in foraminiferal calcite followed the initial protocol of Barker et al. (2003), but included a reductive cleaning step according to Martin and Lea (2002). Foraminiferal shells were dissolved in weak nitric acid, and elemental analyses were carried out on the axial viewing Varian 720 inductively coupled plasma optical emission spectrometry (ICP-OES) at GEOMAR. In order to detect possible drifts of the ICP-OES during analyses, dilution of sample solution with yttrium water (concentration: 112.5 µmol/L) was performed prior to measurement. The ECRM 752-1 standard (3.761 mmol/mol Mg/Ca; Greaves et al., 2008) was used as an internal consistency standard, to which all measurements were standardised and trend-corrected. The external reproducibility for the ECRM standard for Mg/Ca is ±0.1 mmol/mol (2σ). Replicate measurements run during different sessions reveal a reproducibility of maximum ~0.2 mmol/mol (2σ). Post-depositional contamination (Rosenthal et al., 2000) was checked in all samples by monitoring their Fe/Ca, Al/Ca, Mn/Ca and Fe/Mg ratios. For most of the samples, Mn/Ca ratios were below 0.1 mmol/mol. The Al/Ca and Fe/Ca are higher than the threshold of 0.1 mmol/mol given by Barker et al. (2003). The Fe/Mg ratios are commonly below 0.05 mmol/mol. Barker et al. (2003) commonly rejected samples with Fe/Mg ratios of >0.1 mol/mol as potentially significantly contaminated by silicate phases. Furthermore, as the Al/Ca, Fe/Ca, Mn/Ca and Fe/Mg ratios do not correlate with the Mg/Ca ratios (R = 0.18; R = 0.27; R = 0.29; R = 0.08, respectively), we consider sample contamination negligible for our Mg/Ca analyses.

Mg/Ca ratios of *G. ruber* (pink) were converted into SST ($SST_{Mg/Ca}$) using the 'warm water' multispecies calibration and the 'species specific' calibration of Anand et al. (2003). For consistency, all Mg/Ca ratios presented in this study (own data and reference data sets, for example, Schmidt et al., 2012) were transferred into temperatures using the abovementioned calibrations. The assumed habitat depth of *G. ruber* is ~30 m water depth. For the interpretation of our $SST_{Mg/Ca}$ records derived from *G. ruber* (pink), we acknowledge a seasonal bias of the abundance maximum towards the boreal summer months. A calculated top core $SST_{Mg/Ca}$ of *c.* 30°C (30.18°C) is slightly higher than modern temperatures in the AJP of 26.1–28.3°C (Levitus et al., 1994; World

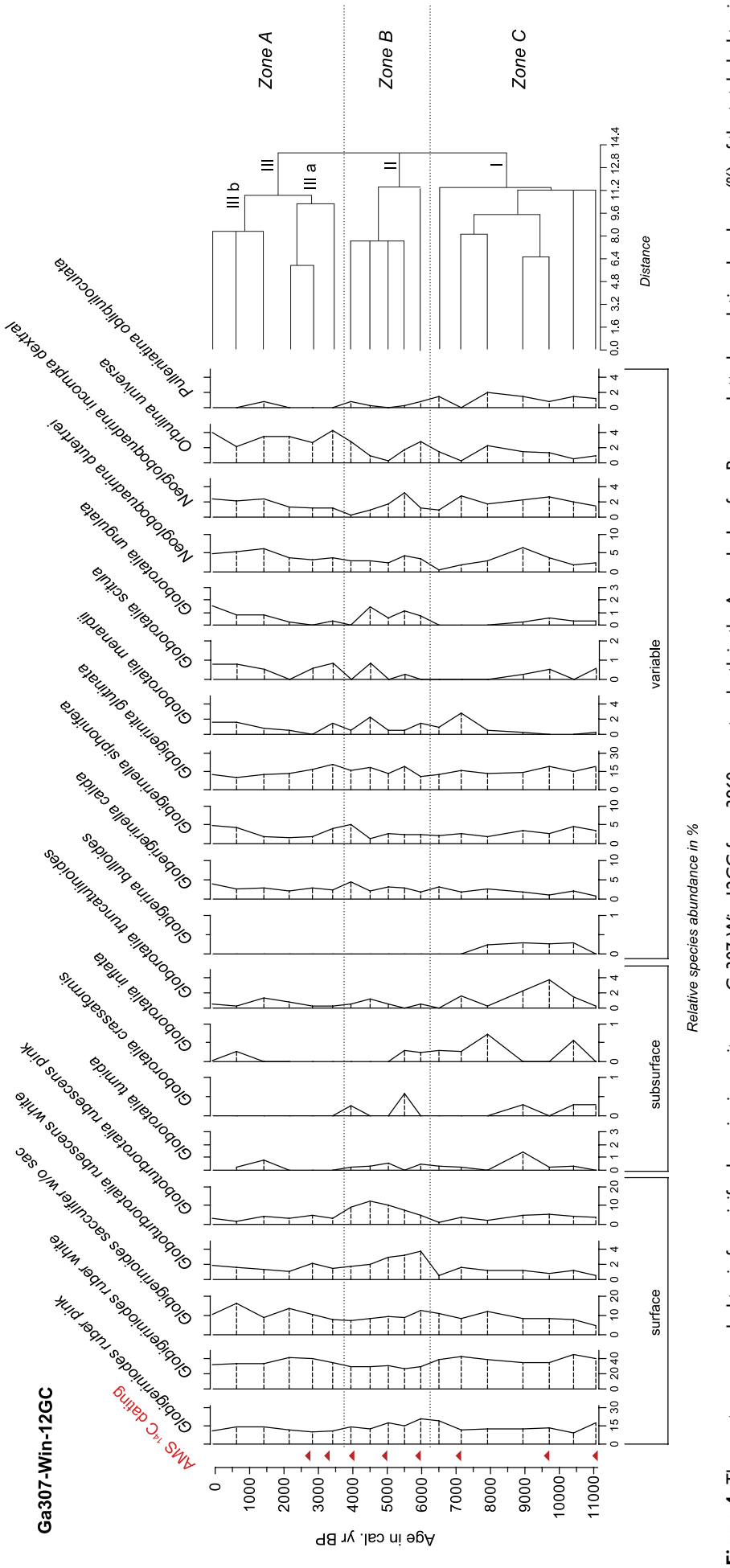

Figure 4. The most common planktonic foraminiferal species in gravity core Ga307-Win-12GC from 3960 m water depth in the Anegada–Jungfern Passage plotted as relative abundance (%) of the total planktonic foraminiferal fauna. Zones A, B and C are defined according to clusters I, II and III based on a constrained cluster analyse. The subcluster IIIa and IIIb are shown.

Ocean Atlas, 1998; Figure 2). As expected, it points towards a summer bias in the $SST_{Mg/Ca}$, but also suggest that the calculated $SST_{Mg/Ca}$ may be slightly too high. This is in accordance to previous studies, as *G. ruber* (pink) generally lives at warmer and shallower water depths than *G. ruber* (white; see Regenberg et al., 2009) and has a bias towards warmer seasons (Haarmann et al., 2011; Richey et al., 2012) and hence is higher in Mg/Ca. Within this context, it is also notable that for *G. ruber* (pink), a positive relationship has been found of increasing 1.1 mmol/mol (~2.5°C) from the smallest (150–212 μm) to the largest (>500 μm) size fractions (Richey et al., 2012). The latter authors report that this is not the case for *G. ruber* (white). In addition, some general uncertainty in the $SST_{Mg/Ca}$ should be assumed, likely in the range of ~±0.5–1°C (e.g. Bahr et al., 2011; Nürnberg, 2015; Regenberg et al., 2009).

Within this context, it must be noted that depending on the oceanographic setting, the Mg/Ca–temperature relationship can be complicated by preferential Mg dissolution (e.g. Elderfield and Ganssen, 2000; Regenberg et al., 2006), post-depositional Mg/Ca enrichment (Regenberg et al., 2007) and the effect of significant salinity change (Nürnberg et al., 1996). Regenberg et al. (2007) in fact showed that diagenetic alteration takes place in the Windward Passage at time scales of >100 kyr, but such a diagenetic effect has not previously been seen at shorter timescales in our region. In addition, dissolution, which would lower $SST_{Mg/Ca}$, does not likely play a role in the area because of high aragonite preservation (Nürnberg et al., 2008). Evans et al. (2016) found a coherent relationship between Mg/Ca and the carbonate system. They argue that pH rather than the HCO_3^{2-} may be the dominant control. Anomalously, high salinity at our coring sites is therefore a potential factor to be considered when assessing the generated (too high) SST maxima. Not only high surface salinity but also in situ seabed impact by dense, ultra-high salinity waters reported to originate from the Salt River Estuary on St Croix (Figure 3a) under hurricane passages cascading down the Salt River Canyon (Figure 3a; Hubbard, 1992) must be taken here into account. Waters from the Salt River (mangrove) Estuary at the head of the canyon have salinities of up to 37 psu (Kendall et al., 2005). The presence of a large, deep sediment fan of the Salt River Bay (Kuijpers and Project Group, 2007) confirms the important role of turbidity flow processes affecting the estuary and canyon area under gale-force wind conditions. The isotope data do, however, not show clear concurrent variations.

Results

Planktonic foraminiferal distribution

A total of 33 planktonic foraminiferal taxa were recorded in the two cores (Table 2). The species *G. ruber* (pink and white variety), *G. sacculifer* w/o sac and *G. glutinata* strongly dominate the assemblage, as expected for tropical/subtropical environments (Figures 4 and 5). Superimposed on the general dominance of these species, the records show small, but consistent, downcore variations in the abundance of subtropical species and deeper dwelling (subsurface) species. In gravity core Ga307-Win-12GC (Figure 4), the subsurface dwelling species *G. crassaformis, G. inflata, G. truncatulinoides* and *G. tumida* are present in the lower part of the core (maximum abundances at 100–70 cm core depth; 11,130–7500 cal. yr BP) with relative abundances between 1% and 4%. The surface dwellers *G. ruber* and *G. rubescens* increase in relative abundance in the mid part of the core section (60–25 cm; 6900–3700 cal. yr BP), while the species *G. sacculifer* w/o sac, *Orbulina universa, N. dutertrei* and *N. incompta* dextral reach maximum abundances in the uppermost part of the core (20–0 cm; 2000–0 cal. yr BP). The fauna in box core Ga307-Win-02BC (Figure 5) shows a similar faunal distribution, which particularly applies to the increase in subsurface dwellers *G. truncatulinoides* and *G. tumida*, being most prominent in the upper part of the core (10–0 cm; 1500–0 cal. yr BP).

A comparison of the total abundances of surface and subsurface species shows an overall dominance of surface dwelling species in both cores (Figure 6a and b). With 65–75%, the relative abundance of surface water species is slightly higher in core Ga307-Win-02BC, which is located closest to the island of St Croix, when compared with 55–65% relative abundance of surface dwellers in core Ga307-Win-12GC located further off-shore (Figure 2a). The subsurface community is limited to a relative abundance of 0.3–4% in both cores, reaching a maximum between 0–1800 and 8000–10,000 cal. yr BP. The remaining fraction of the assemblage is made up of species with variable or unknown depth requirements.

Statistical analyses

The Q-mode constrained cluster analysis of planktonic foraminiferal assemblages in core Ga307-Win-12GC, comprising 18 samples, resulted in three clusters, termed I, II and III, used to define the planktonic foraminiferal zones A, B and C (Figure 4). Cluster I consists of seven samples in the lower part of the core section (Zone A: core depth = 100–55 cm; 11,129–6580 cal. yr BP), cluster II includes the assemblages of five samples in 50–30 cm core depth (Zone B: 6033–4007 cal. yr BP), whereas the top of the core (Zone C: 25–0 cm; 3463–0 cal. yr BP) forms cluster III, comprising six samples. These clusters were used to establish the faunal zonation of the core (Figure 4).

The scores of a Q-mode constrained cluster analysis of the box core Ga307-Win-02BC did not show the presence of distinct clusters during the last 5400 cal. yr BP covered by this core. As the partitioning into clusters for core Ga307-Win-02BC is less clear, we instead highlight where the faunal boundaries established for core Ga307-Win-12GC would be found in core Ga307-Win-02BC (Figure 5). Although the adopted zonation correlates with a change in sedimentation rate reflecting a shift in sediment dynamics, the foraminiferal fauna reveals only minor changes, which suggests a possible change in circulation intensity rather than a major shift in water mass.

SST, oxygen isotopes and Mg/Ca–temperature values

The SST reconstructions based on the ANN transfer functions were calculated as summer, winter and annual averages. Summer and winter SSTs are plotted in Figure 6c and d, respectively. Summer SSTs vary from 28.4°C to 29.5°C for the off-shore core Ga307-Win-12GC and 28.2–29.1°C for the near-shore Ga307-Win-02BC (outlier in this core: T = 27.5°C). The winter SST reconstruction shows SSTs ranging between 25.5°C and 27°C for the near-shore core Ga307-Win-02BC and 25.7–27°C in the gravity core Ga307-Win-12GC. The calculated temperature range is similar to modern temperatures in the AJP, which vary between 26.1°C and 28.3°C with an annual average of SST = 27.4°C (Levitus et al., 1994; World Ocean Atlas, 1998). CTD measurements showed a surface temperature of 26.8°C in March 2007 (Figure 2b). A trend of relatively cooler temperatures (winter SST_{ANN}) is observed in the lower part of the gravity core (100–60 cm core depth; Zone C), while the overall trend in the summer SST_{ANN} is very weak, but with a very slight trend towards cooler condition in Zone B than in Zones A and C.

In comparison with the ANN-based SST reconstruction, the Mg/Ca-derived temperature record ($SST_{Mg/Ca}$) performed on *G. ruber* (pink) displays somewhat higher maximum values that are concentrated in the 30.0–31.0°C range, with one outlier at 32.2°C (Figure 6e). As outlined above, this difference may be because of the (Salt River Canyon) salinity effect on this site. As discussed above, the $SST_{Mg/Ca}$ on *G. ruber* may be biased towards summer

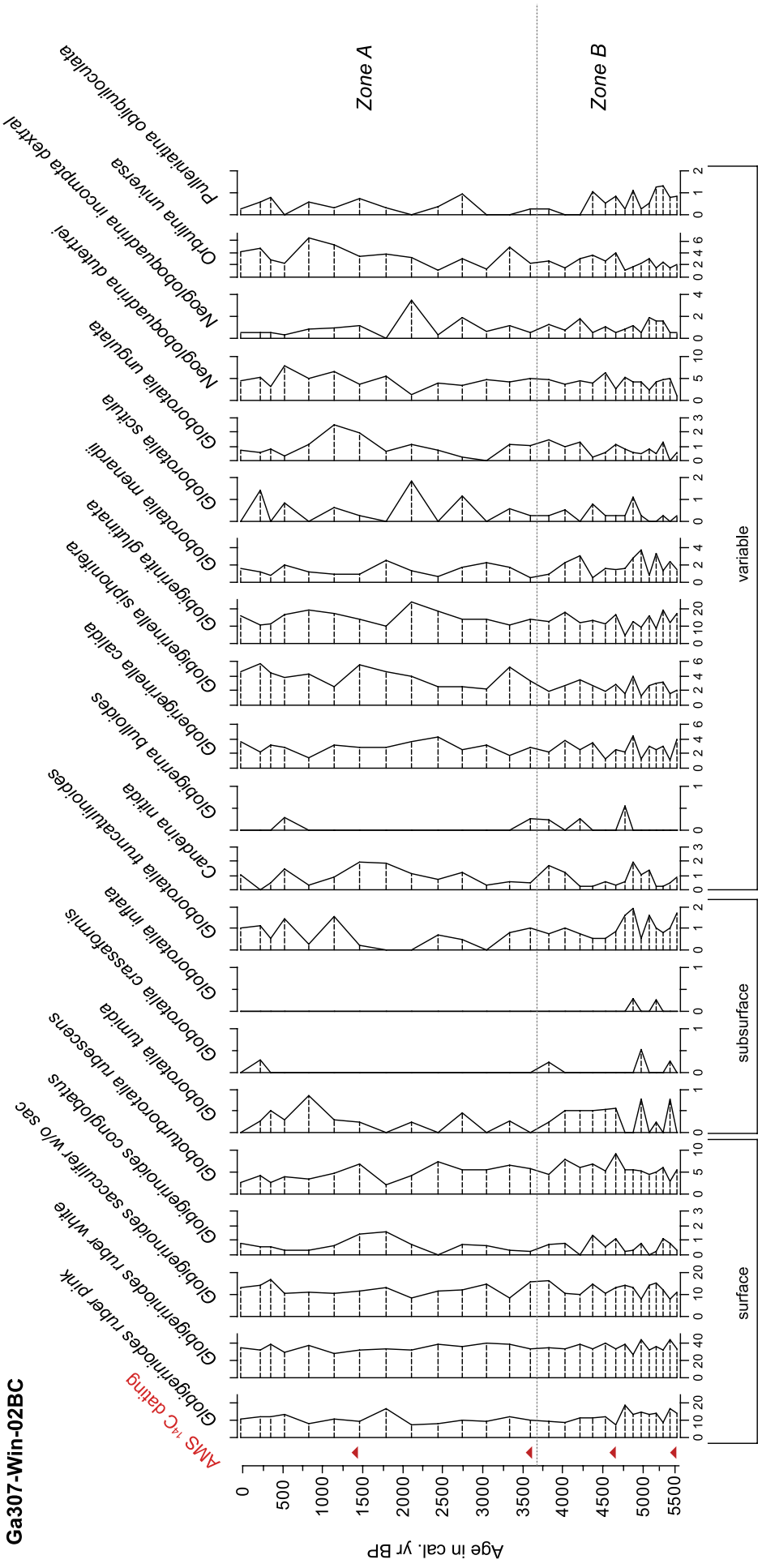

Figure 5. Planktonic foraminiferal assemblage in box core Ga307-Win-02BC, retrieved from 1026 m water depth in the Anegada–Jungfern Passage, showing the most abundant species. Relative abundances were calculated in percentage of the total planktonic foraminiferal fauna. The indication of zones B and C is adopted from the cluster analysis of the gravity core Ga307-Win-12GC.

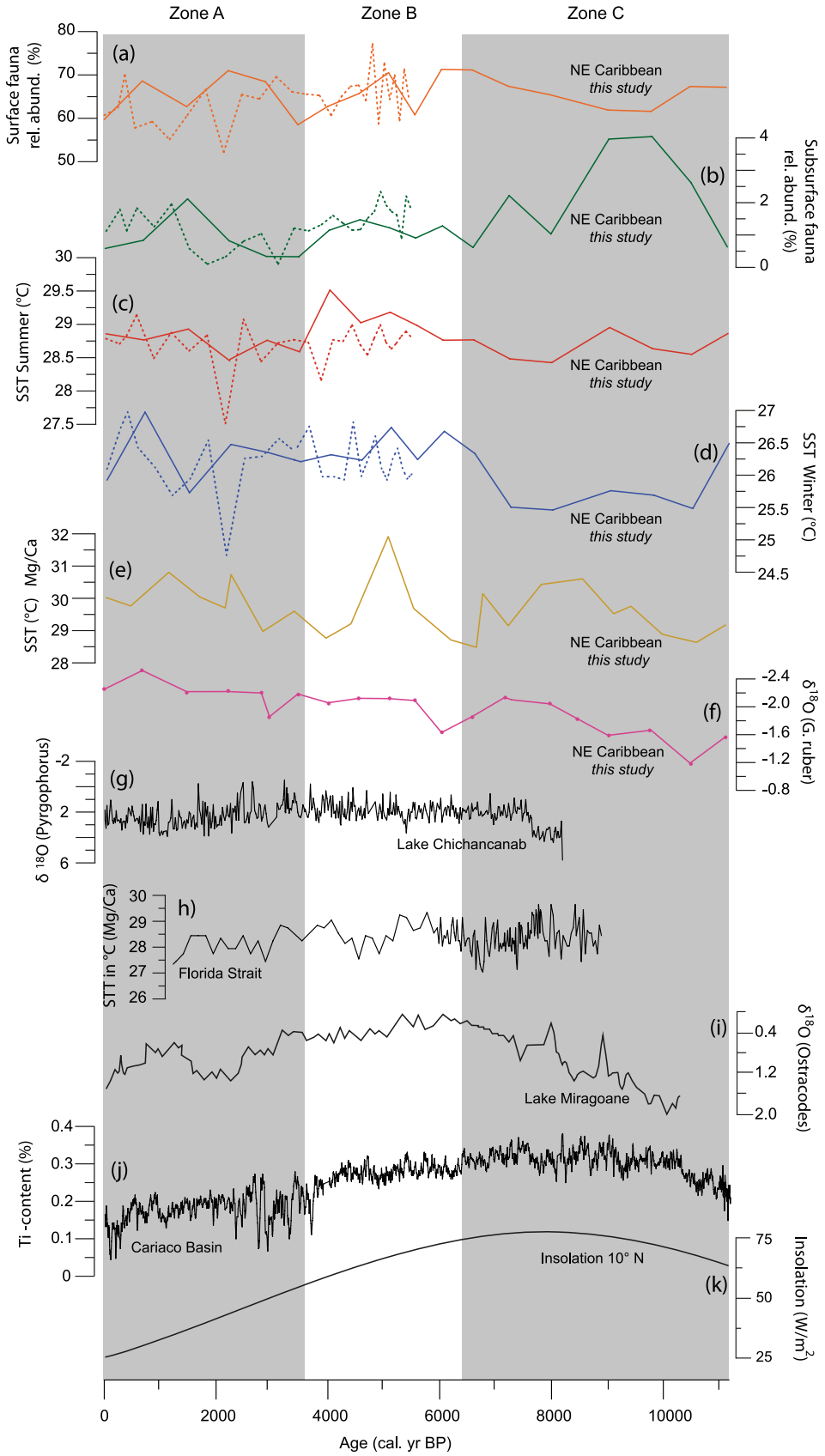

Figure 6. Climate proxy records from the Caribbean area, including zones A, B and C based on the record of this study. Curves (a)–(f) are the climate proxies from core Ga307-Win-12GC, dashed line: core Ga307-Win-02BC – (a) relative abundance of the surface dwelling planktonic foraminiferal assemblage; (b) distribution of the subsurface planktonic foraminiferal assemblage; (c) summer sea-surface temperature (SST) based on ANN transfer function calculations; (d) winter SST based on the ANN transfer function; (e) planktonic $\delta^{18}O$ measured on *Globigerinoides ruber* (pink) from core Ga307-Win-12GC; (f) Mg/Ca-derived SST values from *G. ruber* (pink) (note anomalously high maxima, see also Figure 6c); (g) $\delta^{18}O$ on *Pyrgophorus* sp. in Lake Chichancanab, Mexico (from Hodell et al., 1991); (h) sea-surface temperature based on Mg/Ca of *G. ruber* white from marine sediment core KNR166-2JPC51, Florida Strait (from Schmidt et al., 2012); (i) ostracod $\delta^{18}O$ from Lake Miragoane, Haiti (Hodell et al., 1991); (j) Titanium content from ODP Site 1002, Cariaco Basin (from Haug et al., 2001); and (k) insolation curve for 10°N based on Berger (1978; from Fensterer et al., 2013).

conditions; however, overall, the $SST_{Mg/Ca}$ does now show a clear pattern of the slight warming seen in Zone B in the summer SST_{ANN}, when disregarding the one sample with very high temperatures. Overall, the variability in the record is too high to pinpoint a clear pattern.

Oxygen isotope values ($\delta^{18}O$), retrieved for the gravity core Ga307-Win-12GC on the surface dweller *G. ruber* (pink), vary between −2.4‰ and −1.0‰, with the highest values observed in the older part of the core (100–60 cm) and decreasing towards the present (Figure 6f).

Discussion

Signal versus noise

An important oceanographic feature of the Caribbean region is the small, seasonal and inter-annual temperature changes in ocean surface waters. Consequently, variations in planktonic foraminiferal assemblages, SST and oxygen isotopes values are all very small, with the range of variations in SST and $\delta^{18}O$ generally being within the predicted method errors and uncertainties. Even between glacial and interglacial climate conditions, Caribbean SST differences do not exceed 3.5°C (Barker et al., 2005). This highlights the difficulties in interpreting potential changes in tropical ocean conditions during an overall warm period such as the Holocene, as it is very difficult to distinguish between noise and signal.

The results from the ANN-based temperature reconstruction for both summer and winter SSTs display precisely the same range as found by Nyberg et al. (2002) for Caribbean waters in the south of Puerto Rico where the latter authors compared and measured the ANN-derived surface water temperatures. Moreover, the reconstructed SST range also agrees with temperature results derived from sclerosponges Sr/Ca ratios and oxygen isotope analyses obtained for the 'Little Ice Age' period (Haase-Schramm et al., 2003). The Mg/Ca-derived temperature range based on the calibration methods of Anand et al. (2003), shows somewhat larger amplitudes (*c*. 4°C). The SST temperature maxima appear somewhat beyond observational values, which we tentatively explain by the influence of ultra-high salinity of ambient waters originating from the St Croix Salt River estuary combined with an effect of the generally relatively high temperatures derived from Mg/Ca on *G. ruber* (pink; Haarmann et al., 2011). Nevertheless, also the Mg/Ca record shows rather subtle changes of 1–2°C during much of the record if the extreme peak in mid Zone B is disregarded as a outlier. In a tropical environment, any change in SST and sea-surface salinity is, however, quite minor and will thus only have a very subtle signal, especially during a generally warm climate period (interglacial) such as the Holocene. This will also have an effect on the biological community, in this case illustrated by only minor variations in the planktonic foraminiferal community.

Therefore, when considering records from the tropics, it is especially important to evaluate signal versus noise. Here, we will disregard smaller fluctuations covering less than four data points (corresponding to a time span of a few thousand years), which we consider likely to be noise. Moreover, only changes consistently found in all relevant proxies have been used for the final conclusions. This means that despite the only relatively small differences in value between 'low' and 'high', the consistent, long-term pattern is useful, not the least when several proxies indicate a similar pattern. Thus, we argue that even though each method provides results within or close to the statistical uncertainly, if all proxies give the same pattern, results may be considered reliable. Within this context, we also underline that our results refer to long-term oceanographic changes at multi-centennial to millennial time scale.

Palaeoceanographic development of the AJP in relation to North Atlantic climate

Consequently, we use the overall signal of these persistent, albeit generally small, changes in the planktonic foraminiferal faunas, SST and geochemistry to discuss the overall palaeoceanographic and palaeoclimatic changes occurring in the northeastern Caribbean during the last ~11,100 cal. years (for a general overview, see summary in Table 3).

The planktonic foraminiferal assemblages are dominated by the surface dwelling species *G. ruber* and *G. sacculifer*, as well as *G. glutinata*, which can be found at various depths, in all samples of both cores. This reflects overall warm, tropical to subtropical, surface water conditions persisting in the AJP during the entire Holocene. Today, highest concentrations of *N. dutertrei* and *G. glutinata* are in the northeastern Caribbean Sea, while in the Anegada Passage, where Sargasso Sea water flows into the Caribbean Sea, lower standing stocks indicate more oligotrophic conditions. In contrast, the SUW masses entering the Caribbean Sea through the Anegada Passage in water depths between 100 and 300 m are characterised by higher concentrations of the subsurface dweller *G. truncatulinoides* compared with the adjacent water masses. High abundance of particularly *G. glutinata*, which is often found in connection to cyclonic eddies and thus strong mixing (Schmuker and Schiebel, 2002) both at present and in the fossil record at our site, is in support of the overall only small changes seen in our Holocene faunal assemblages and in SST (i.e. ANN-based temperature variation within 1.5°C). It should, however, be noted that the SST reconstructions based on ANN transfer functions are calibrated to a water depth of 10 m, which is not necessarily the water depth where most of the variances caused by oceanographic changes are expected (Telford et al., 2013). In fact, a study of historical hydrographic changes in the Caribbean Sea demonstrates that changes are most pronounced at greater subsurface depths below 100 m (Jury, 2011). Hence, changes deeper down in the water column may have been much more pronounced than indicated by the present SST estimates.

The cluster analysis underlines that at a multi-centennial to millennial scale small, but still important changes occurred in the oceanographic setting of the Holocene. Defined by core Ga307-Win-12GC, the clusters I, II and III (Figure 4) reveal three Holocene oceanographic stages in the AJP. Additional information is provided by core Ga307-Win-02BC from shallower water depth, providing a higher resolution for the past 5400 years.

Zone C: 11,100–6300 cal. yr BP. Beside the dominance of the (sub)tropical surface dwellers (see above), this period is marked by the relative small, but consistent presence of species belonging to the subsurface community (Figure 6a and b). In studies from tropical and subtropical realms (e.g. Birch et al., 2013; Mulitza et al., 1997; Schmidt et al., 2012; Schmuker and Schiebel, 2002), deep-to-intermediate dwelling (subsurface) species such as *G. crassaformis* and *G. truncatulinoides* may be used to identify the influence of cooler, subsurface waters in the upper part of the water column, which implies a relatively shallow position of the thermocline. In the AJP, where the thermocline is found at the SUW depth stratum below the CSW, these deep-to-intermediate dwellers indicate the presence of a relatively shallow (<100 m) thermocline. Since a relatively shallow position of the thermocline would today be linked to relatively strong mixing of AAIW and SUW, the shallow thermocline observed in our record indicates a relatively strong inflow of SUW and AAIW into the AJP, although trade-wind-induced strong upwelling on a more local scale may also have played a role (see below; Table 3). Moreover, the presence of the, in the tropics, cool upwelling species *G. bulloides* in the oldest *c*. 400 year part of the record points to the presence of cooler water masses derived from upwelling areas.

Table 3. Simplified overview of climatic and oceanographic conditions affecting the Anegada–Jungfern Passage, inferred from our data in context of previous studies of large-scale circulation patterns.

Time (cal. yr BP)	Planktonic foraminiferal assemblages	SST (winter)	SST (summer)	Surface water	Subsurface waters	Intermediate water	Thermocline	South Atlantic Subtropical Gyre	AMOC	ITCZ	Trade winds
0–3700	Increase in tropical surface dwellers	≈ Similar to today	≈ Similar to today	Strong CSW and SUW mixing Stable stratified upper water column Reduced upwelling		Weak inflow of AAIW	Deep	Weaker	More variable; overall relatively weak	Moving close to present position	≈ Similar to today
3700–6300	Fewer subsurface dwellers	Warming of surface waters	≈ Similar to today	Vertical expansion of CSW Reduced upwelling	Downward expansion of SUW	AAIW inflow decreasing	Deep	Weaker	Weaker	Migrating southward	Weaker
6300–11,100	Consistent presence of subsurface dwellers	Cool surface waters	≈ Similar to today	Relatively thin layer of CSW Good ventilation Upwelling	Strong inflow of SUW Relatively strong mixing of AAIW and SUW	Strong inflow of AAIW	Shallow	Strong	Strong	North of present position	Strong

SST: sea-surface temperature; AMOC: Atlantic Meridional Overturning Circulation; ITCZ: inter-tropical convergence zone; CSW: Caribbean surface water (modern – down to 25–100 m water depth); AAIW: Antarctic Intermediate Water (500–1000 m water depth); SUW: subtropical underwater (50–180 m below sea surface today).

A stronger-than-present influence of AAIW may have been linked to an intensified South Atlantic Subtropical Gyre and a generally strong AMOC (Knudsen et al., 2011; Lynch-Stieglitz et al., 2009; Schmidt et al., 2004), favouring water mass transport from the wider Atlantic region towards the Caribbean. This would have resulted in an overall stronger ventilation of surface, as well as subsurface and intermediate water masses, through the Caribbean Sea and the Gulf of Mexico. An intensified Loop Current strength has in fact been observed between 9000 and 6000 cal. yr BP (Poore et al., 2004; Schmidt et al., 2012). Moreover, an enhanced subtropical gyre circulation during this period has also been reported from the Gulf Stream region (Cléroux et al., 2012).

In addition to the higher ratio of subsurface dwelling species (Figure 6b), the ANN temperature approximation shows slightly, but persistently, cooler winter SSTs (25.5°C) than today (Figure 6c and d). These lower-than-present winter SSTs are in agreement with the relatively cool SST observed in the Florida Strait during this time period (Figure 6h), reaching a maximum cooling at 6900 cal. yr BP (Schmidt et al., 2012). The stronger-than-present seasonality in the Caribbean, illustrated by our cooler winter SST records combined with summer SSTs more similar to today, is likely linked to the solar insolation record, causing a maximum in Northern Hemisphere summer solar insolation and a minimum in winter insolation in the early-Holocene (Imbrie et al., 1989; Ruddimann, 2003). At 10°N in the Caribbean, the minimum (maximum) in winter (summer) solar irradiation (Figure 6k) is reported to occur between 8000 and 6000 cal. yr BP (Berger, 1978; Hodell et al., 1991), which is in good agreement with the relatively low winter SST seen in the AJP.

It is important to note that the early-Holocene solar insolation pattern is believed to have resulted in a northward shift of the annual position of the ITCZ compared with the present situation (Haug et al., 2001; Hodell et al., 1991; Knudsen et al., 2011; Koutavas and Lynch-Stieglitz, 2004; Schneider et al., 2014; see also Figure 6f–j). This presumably caused a generally strong trade wind regime (Caribbean Low Level Jet) and a positive evaporation/precipitation ratio in the northern Caribbean (cf. Wang, 2007), favouring upwelling leading to a shallowing of the thermocline and surface water cooling. Also, a scenario of a more northerly ITCZ position would have led to a northward expansion of the Guyana coastal upwelling zone in the NE of South America, resulting in cooling of upper water masses that are transported north into the Caribbean region, thus explaining that summer surface water temperatures were not warmer than present despite the higher summer solar insolation. More generally, the energy balance between Northern and Southern Hemispheres can be concluded to be the main factor controlling migration and dynamics of the ITCZ (Schneider et al., 2014).

Zone B: 6300 – 3700 cal. yr BP. The reduction in subsurface dwellers in the planktonic foraminiferal assemblage after 6300 cal. yr BP suggests a deepening of the thermocline implying a thickening of the warmer surface water layer. These conditions would have favoured surface dwelling species, as also supported by the increased frequencies of the tropical surface dwellers *G. ruber* pink and *G. rubescens* (pink and white). A general trend of relative sea-surface warming seen both in the winter SST_{ANN} data (ANN winter $\Delta T = +0.8$°C) and nearly unchanged summer SSTs indicates a weaker seasonality and stabilisation/warming of the surface stratum (Table 3). A similar surface warming is also seen in the Florida Strait between 6300 and 5000 cal. yr BP, indicated by Mg/Ca-based SST approximation (Schmidt et al., 2012; Figure 6g).

The deepening of the thermocline suggests a reduced inflow of cooler, intermediate waters and weaker trade-wind-induced upwelling in the study area. The flow of AAIW into the Caribbean may have been reduced due to a weakening of the AMOC, as

previously suggested by Rühlemann et al. (1999) (Table 3). More specifically, a gradual southward migration of the ITCZ must have led to a corresponding shift in the southeast trade wind belt, contributing to a decrease in advection of cooler (sub)surface water masses from the Guyana upwelling region. These conditions may have favoured expansion of the warmer surface and subsurface water masses (CSW and SUW) in the AJP, most prominently between 6300 and 4500 cal. yr BP.

As discussed above, our SST estimations indicate that surface water conditions were seasonally more stable than during the early-Holocene, possibly because of the smaller differences in summer versus winter solar insolation (Imbrie et al., 1989; Ruddimann, 2003). The resulting weaker atmospheric pressure gradient and equator-wards migration of the summer position of the ITCZ during the mid-Holocene (Haug et al., 2001; Knudsen et al., 2011; Ruddimann, 2003; Schneider et al., 2014) are thought to have favoured both more annually stable SST and more prevalent humid climate conditions in the Caribbean area (Curtis and Hodell, 1993; Fritz et al., 2011; Hodell et al., 1991, 1995). At the same time, regional trade wind activity can be assumed to have weakened. This may also have contributed to slightly warmer winter SST values found in the Gulf of Mexico during that time (Poore et al., 2003). Moreover, upper water mixing related to warm season hurricane activity was also reduced as can be concluded from low hurricane activity over the northeastern Caribbean during the mid-Holocene (Toomey et al., 2013).

López-Otàlvaro et al. (2009) described a thermocline shoaling and a concentration of warm surface waters from the equatorial Atlantic in the eastern Caribbean, associated with a southward displacement of the ITCZ. A weaker mid-Holocene subtropical gyre circulation after 6500 cal. yr BP has also been documented in a study from the Gulf Stream region (Cléroux et al., 2012). Ocean–atmosphere modelling by Wang (2007) suggests a direct correlation between SST warming, high rainfall intensity and a weak trade wind system in the Caribbean region, conditions reflecting our mid-Holocene circulation regime. Higher precipitation rates at that time are also indicated by coral records from the southeastern part of the Caribbean (Felis et al., 2013), as well as from Caribbean stalagmite and lake records more to the north (Mangini et al., 2007). Increased precipitation over the NE Caribbean islands must have led to a relatively higher sedimentation rate during this period, as indeed is recorded at the near shore core site Ga307-Win-02BC, which is likely more sensitive to insular runoff and associated sediment dispersal than our other coring site further offshore.

Zone A: 3700 cal. yr BP – Present. The late-Holocene in our cores is likewise characterised by dominance of surface dwellers. The clear increase in the tropical surface dweller *G. sacculifer* and the variable *O. universa* combined with the continued high summer and winter SST, suggest warm, stable temperature ($\Delta T_{(\text{summer–winter})} = -0.7$°C; compare Figure 6c and d) conditions in the (CSW) surface water. As photosymbionts, both species suggest a warmer surface water overlying the also quite warm subsurface water masses, indicating a strong surface and subsurface water mixing. The low influx of subsurface dwellers indicates that the thermocline in the AJP continued to be located at greater water depth. This again suggests a still relatively weak inflow of (AAIW) subsurface/intermediate waters (Table 3).

In addition to a potential reduction in inflowing AAIW, the thickening of the warm surface water layer may have been linked to the further expansion of the Atlantic tropical surface water warm pool (López-Otàlvaro et al., 2009; Rühlemann et al., 1999). This would reflect a general weakening of the AMOC, as previously suggested by Zhang (2007), who attributed this to an insolation-forced southward migration of the ITCZ.

The reduced difference between summer and winter SSTs in this period, may, in addition to the general reduction in Northern Hemisphere summer insolation and increase in winter insolation, also be linked to trade wind weakening over the Caribbean during the winter season, causing reduced upwelling. In addition, more common tropical cyclone passages with their wind stress and cloud cover may have contributed to summer SST lowering. This conclusion is also supported by studies of shallow marine environments on the nearby island St Croix (Jessen et al., 2008), indicating stronger winds and associated increased wave action between *c*. 4000 and 2200 cal. yr BP. More recently, Toomey et al. (2013) showed an increase in hurricane frequency at the Grand Bahamas Banks after 4400 cal. yr BP, linking this to the decrease in Northern Hemisphere summer solar insolation. Olsen et al. (2012) reported a major shifts towards a more negative NAO pattern in the North Atlantic region after 4200 cal. yr BP, while Haug et al. (2001) suggest an increase in ENSO variability, with the strongest ENSO frequencies between 3500 and 2600 cal. yr BP. Compared with the mid-Holocene, the surface water conditions in the AJP were, generally, likely somewhat less stable and slightly cooler during the last *c*. 4000 years. This is also supported by near annually resolved planktonic foraminiferal oxygen isotope records from the southeastern Caribbean Sea indicating up to 2°C SST cooling and increased upwelling intensity in this region over the last 2000 years (Black et al., 2004).

In addition, during the last 2000 cal. yr BP, a small increase in *N. dutertrei, G. ungulata* and *G. siphonifera* that are found at varying depths, but often linked to subsurface waters, indicates a shift in the (sub)surface inflow, which is coeval with subtropical gyre circulation changes observed in the Gulf Stream region (Cléroux et al., 2012). The latter two species are described to inhabit lower levels of the surface water stratum, preferably following the chlorophyll maximum (Birch et al., 2013). Although the change in fauna is only very minor, in combination with the presence of the sub-thermocline species *G. scitula* (Birch et al., 2013), this suggests a slight shallowing of the thermocline. Interestingly, the timing of our minor faunal change (within Zone A) coincides with a shift to a more frequently negative NAO pattern prevailing over the North Atlantic (Jessen et al., 2011; Olsen et al., 2012; Seidenkrantz et al., 2008). Here, it should be noted that SST warming in the eastern Equatorial Atlantic appears to be correlated to a negative NAO index (Joyce et al., 2000), which implies that under a persisting negative NAO regime, anomalously, warm surface water from the eastern Equatorial Atlantic can reach the eastern Caribbean. Such a scenario appears to have been the case, as is indicated by the high values of the Mg/Ca SST profile recorded for the past 2000 years (Figure 6f). A shift in Eastern North Atlantic Central Water hydrography recorded between 3300 and 2600 cal. yr BP illustrates a transition towards enhanced mid-latitude atmospheric circulation in particular during cold events (Morley et al., 2014). Correspondingly, at the same time, the NE Caribbean climate experienced a trend towards warmer and more variable humid conditions (Fritz et al., 2011; Higuera-Gundy et al., 1999; Hodell et al., 1991). Our records show no clear evidence of the global cooling SST trend described for the last 2000 years by McGregor et al. (2015), but resolution may be too low to allow such a comparison.

Conclusion

Using qualitative and quantitative analyses of planktonic foraminifera assemblages, $\delta^{18}O$ proxy and Mg/Ca–temperature relationship (*G. ruber* pink), as well as SST derived from ANN transfer functions, a reconstruction was made of the upper water mass variability in the AJP, northeastern Caribbean Sea, over the last *c*. 11,100 years (Figure 6; Table 3). Our data indicate overall warm conditions throughout the Holocene. Small, but consistent, changes in the planktonic foraminiferal assemblages and SST have been used to trace variations in water mass distribution and

advection in the NE Caribbean. Only absolute ANN-derived SST values have been discussed. Some of the Mg/Ca-based temperature estimates display anomalously high maxima, but overall trends confirm the Holocene variations observed in the ANN-derived SST record. Recent instrumental data from this region document that such small variations in surface water conditions signal more prominent hydrographic changes at greater (>100 m) subsurface depth.

In the early- to mid-Holocene (11,100–6300 cal. yr BP), the planktonic foraminiferal assemblages indicate a shallow thermocline and expansion of subsurface water masses (AAIW). A northward displaced ITCZ with a pronounced seasonality in early-Holocene tropical solar insolation may have contributed to increased trade-wind-forced transport of surface water masses (CSW) and advection of southern-source subsurface waters from the seasonal upwelling areas off the South American coast.

In the mid-Holocene (6300–3700 cal. yr BP), the planktonic foraminiferal fauna suggests a deepening of the thermocline zone and an expansion of the tropical warm water pool in the NE Caribbean. Relatively high and stable SSTs with only small, seasonal variations may be related to a decrease in trade wind activity associated with the southward migration of the ITCZ.

The late-Holocene palaeoceanographic regime shows a continuation of relatively stable stratified upper water mass and minor SST variations. With a further southward migration of the ITCZ, the influence of the North Atlantic Subtropical Gyre extended further south, favouring flow of stable, warm and saline waters (SUW) into the eastern Caribbean. At the same time, SST variability and seasonality further decreased. A minor change in upper water mass conditions with a slight SST increase during the past 2000 years may be related to a change in large-scale atmospheric circulation over the North Atlantic, where meridional circulation patterns appeared more frequently.

More generally, it may be concluded that a clear link exists between Caribbean upper water mass conditions and hydrographic conditions in the Gulf Stream sector of the North Atlantic Subtropical Gyre. Relatively low SST in the northeastern Caribbean appears to be correlated to enhanced Gulf Stream activity and vice versa. The large-scale circulation regime of this entire region can be concluded to depend mainly on the position of the ITCZ, which in turn reflects the inter-hemispheric atmosphere energy balance.

Acknowledgements

The Danish Expedition Fund is thanked for organising the 'Galathea3 Around-the-World Expedition', of which this study benefitted from 'Leg 16'. Roy A. Watlington, Professor Emeritus at the Department of Marine Sciences of the University of the Virgin Islands, St Thomas, is gratefully acknowledged for his support and efforts in helping to run the field work and cruise of the 'WINMARGIN' project successfully. The captain and crew on board HMS '*Vædderen*' are thanked for their assistance during cruise Leg 16 of the Galathea3 Expedition in March 2007. The authors also thank the following persons: Christof Pearce, Aarhus University, for his help applying the age models and for graphical support; Grethe Storgaard, Aarhus University, for her help and suggestions for using graphic programmes; Erik Thomsen, Aarhus University, for useful discussions regarding the application of multivariate statistical analyses; Jesper Find, Aarhus University, for his help in picking specimens for geochemical analyses; Delia Oppo and Dorinda Ostermann at the Woods Hole Oceanographic Institution, US, for measuring stable isotopes of *G. ruber*; and Nadine Gehre at GEOMAR, Germany, for assistance in the Mg/Ca analyses.

Funding

This study was funded by the Danish Council for Independent Research, Natural Science (TROPOLINK grant no. 09/069833-FNU and OCEANHEAT grant no. 12-126709/FNU) and the EU FP7 project PAST4FUTURE (project no. 243908). Furthermore, the WINMARGIN project, during which the cores were collected, would not have been possible without funding by the Villum Kann Rasmussen Foundation (Denmark), with additional support received from Aarhus University and GEUS. The Danish Expedition Fund is thanked for funding the 'Galathea3 Around-the-World Expedition'.

References

Anand P, Elderfield H and Conte MH (2003) Calibration of Mg/Ca thermometry in planktonic foraminifera from a sediment trap time series. *Paleoceanography* 18: 28–31.

Arbuszewski JA, deMenocal PB, Cléroux C et al. (2013) Meridional shifts of the Atlantic intertropical convergence zone since the Last Glacial Maximum. *Nature Geoscience* 6: 959–962.

Bahr A, Nürnberg D, Schönfeld J et al. (2011) Hydrological variability in Florida Straits during Marine Isotope Stage 5 cold events. *Paleoceanography* 26: PA2214.

Barker S, Cacho I, Benway H et al. (2005) Planktonic foraminiferal Mg/Ca as a proxy for past oceanic temperatures: A methodological overview and data compilation for the Last Glacial Maximum. *Quaternary Science Reviews* 24: 821–834.

Barker S, Greaves M and Elderfield H (2003) A study of cleaning procedures used for foraminiferal Mg/Ca paleothermometry. *Geochemistry, Geophysics, Geosystems* 4: 8407.

Bé AWH (1959) Ecology of recent planktonic foraminifera. Part I – Areal distribution in the western North Atlantic. *Micropaleontology* 58: 13–30.

Bé AWH (1967) *Foraminifera families: Globigerinidae and Globorotaliidae* (Contr.nr. 982). Palisades, NY: Lamont Geological Observatory of Columbia University. Available at: http://www.ices.dk/sites/pub/Publication%20Reports/Plankton%20leaflets/SHEET108.PDF.

Bé AWH (1977) An ecological zoogeographical and taxonomic review of recent planktonic foraminifera. In: Ramsay A (ed.) *Oceanic Micropaleontology*. London: Academic Press, pp. 1–100.

Bé AWH and Tolderlund D (1971) *Distribution and Ecology of Living Planktonic Foraminifera in Surface Waters of the Atlantic and Indian Oceans*. Cambridge: Cambridge University Press, pp. 105–149.

Bé AWH, Vilks G and Lott L (1971) Winter distribution of planktonic foraminifera between the Grand banks and the Caribbean. *Micropaleontology* 17: 31–42.

Berger AL (1978) Long-term variations of daily insolation and quaternary climatic changes. *Journal of the Atmospheric Sciences* 35: 2362–2367.

Birch H, Coxall HK, Pearson PN et al. (2013) Planktonic foraminifera stable isotopes and water column structure: Disentangling ecological signals. *Marine Micropaleontology* 101: 127–145.

Blaauw M (2010) Methods and code for 'classical' age-modelling of radiocarbon sequences. *Quaternary Geochronology* 5: 512–518.

Black DE, Thunell RC, Kaplan A et al. (2004) A 2000-year record of Caribbean and tropical North Atlantic hydrographic variability. *Paleoceanography* 19: PA2022.

Boltovskoy E, Boltovskoy D and Brandini F (2000) Planktonic foraminifera from south-western Atlantic epipelagic waters: Abundance, distribution and year-to-year variations. *Journal of the Marine Biological Association of the United Kingdom* 79: 203–213.

Buzas MA (1990) Another look at confidence limits for species proportions. *Journal of Paleontology* 64(5): 842–843.

Cléroux C, Debret M, Cortijo E et al. (2012) High-resolution sea surface temperature reconstruction off Cape Hatteras over the last 10 ka. *Paleoceanography* 27: PA1205. DOI: 10.1029/2011PA002184.

Curtis JH and Hodell DA (1993) An isotopic and trace element study of ostracods from Lake Miragoane, Haiti: A 10,500 year record of paleosalinity and paleotemperature changes in the Caribbean. *Geophysical Monograph Series* 78: 135–152.

Dietrich G (1963) *General Oceanography: An Introduction*. New York: John Wiley & Sons.

Elderfield H and Ganssen G (2000) Past temperature and $\delta^{18}O$ of surface ocean waters inferred from foraminiferal Mg/Ca ratios. *Nature* 405: 442–445.

Evans D, Wade BS, Henehan M et al. (2016) Revisiting carbonate chemistry controls on planktonic foraminifera Mg/Ca: Implications for sea surface temperature and hydrology shifts over the Paleocene-Eocene Thermal Maximum and Eocene-Oligocene transition. *Climate of the Past* 12: 819–835.

Fatela F and Taborda R (2002) Confidence limits of species proportions in microfossil assemblages. *Marine Micropaleontology* 45(2): 169–174.

Felis T, Giry C, Kölling M et al. (2013) Southern Caribbean Sea temperature and salinity variability since the mid-Holocene from monthly resolved coral records. In: *Paper presented to EGU General Assembly 2013*, Vienna, 7–12 April.

Fensterer C, Scholz D, Hoffmann DL et al. (2013) Millenial-scale climate variability during the last 12.5ka recorded in a Caribbean speleothem. *Earth and Planetary Science Letters* 361: 143–151.

Fratantoni D, Zantopp R, Johns W et al. (1997) Updated bathymetry of the Anegada-Jungfern Passage complex and implications for Atlantic inflow to the abyssal Caribbean Sea. *Journal of Marine Research* 55: 847–860.

Fritz SC, Björck S, Rigsby CA et al. (2011) Caribbean hydrological variability during the Holocene as reconstructed from crater lakes on the island of Grenada. *Journal of Quaternary Science* 26(8): 829–838.

Gamble DW and Curtis S (2008) Caribbean precipitation: Review, model and prospect. *Progress in Physical Geography* 32(3): 265–276.

Giannini A, Cane MA and Kushnir Y (2001) Interdecadal changes in the ENSO teleconnections to the Caribbean region and the North Atlantic Oscillation. *Journal of Climate* 14: 2867–2879.

Giannini A, Kushnir Y and Cane MA (2000) Interannual variability of Caribbean Rainfall, ENSO, and the Atlantic Ocean. *Journal of Climate* 13: 297–311.

Gordon AL (1967) Circulation of the Caribbean Sea. *Journal of Geophysical Research* 72: 6207–6233.

Greaves M, Caillon N, Rebaubier H et al. (2008) Interlaboratory comparison study of calibration standards for foraminiferal Mg/Ca thermometry. *Geochemistry, Geophysics, Geosystems* 9: Q08010.

Haarmann T, Hathorne EC, Mohtadi M et al. (2011) Mg/Ca ratios of single planktonic foraminifer shells and the potential to reconstruct the thermal seasonality of the water column. *Paleoceanography* 26: PA3218. DOI: 10.1029/2010PA002091.

Haase-Schramm A, Böhm F, Eisenhauer A et al. (2003) Sr/Ca ratios and oxygen isotopes from sclerosponges: Temperature history of the Caribbean mixed layer and thermocline during the Little Ice Age. *Paleoceanography* 18(3): 1073.

Hammer Ø, Harper DAT and Ryan PD (2001) PAST. Paleontological statistics software package for education and data analysis. *Paleontologia Electronia* 4: 1–9. Available at: http://palaeo-electronica.org/2001_1/past/past.pdf.

Haug G, Hughen K, Sigman D et al. (2001) Southward migration of the Intertropical Convergence Zone through the Holocene. *Science* 293: 1304–1308.

Hemleben C, Spindler M and Anderson O (1989) *Modern Planktonic Foraminifera*. New York: Springer Verlag.

Hernandez-Guerra A and Joyce TM (2000) Water masses and circulation in the surface layers of the Caribbean at 66°W. *Geophysical Research Letters* 27: 3497–3500.

Higuera-Gundy A, Brenner M, Hodell DA et al. (1999) A 10,300 14C yr record of climate and vegetation change from Haiti. *Quaternary Research* 52: 159–170.

Hodell DA, Curtis JH and Brenner M (1995) Possible role of climate in the collapse of Classic Maya civilization. *Nature* 375: 391–394.

Hodell DA, Curtis JH, Jones GA et al. (1991) Reconstruction of Caribbean climate change over the past 10,500 years. *Nature* 352: 790–793.

Hubbard DK (1992) Hurricane-induced sediment transport in open shelf tropical systems – An example from St. Croix, US Virgin Islands. *Journal of Sedimentary Petrology* 62: 946–960.

Imbrie J, McIntyre A and Mix A (1989) Oceanic response to orbital forcing in the late quaternary: observational and experimental strategies. In: Berger AL, Imbrie J, Hays J et al. (ed.) *Climate and Geo-Sciences*. Dordrecht: Kluwer Academic Publication, pp. 121–164.

Inoue M, Handoh IC and Bigg GR (2002) Bimodal distribution of tropical cyclogenesis in the Caribbean: Characteristics and environmental factors. *Journal of Climate* 15: 2897–2905.

Jessen AC, Pedersen JBT, Bartholdy J et al. (2008) A late-Holocene paleoenvironmental record from Altona Bay, St. Croix, US Virgin Islands. *Danish Journal of Geography* 108(2): 59–70.

Jessen CA, Solignac S, Nørgaard-Pedersen N et al. (2011) Exotic pollen as an indicator of variable atmospheric circulation over the Labrador Sea region during the mid to late-Holocene. *Journal of Quaternary Science* 26(3): 286–296.

Johns W, Townsend T, Fratantoni D et al. (2002) On the Atlantic inflow to the Caribbean Sea. *Deep-Sea Research I* 49: 211–243.

Jones J (1967) Significance of distribution of planktonic foraminifera in the Equatorial Atlantic Undercurrent. *Micropaleontology* 13(4): 178–183.

Joyce TM, Deser C and Spall MA (2000) The relation between decadal variability of subtropical mode water and the North Atlantic Oscillation. *Journal of Climate* 13: 2550–2569.

Jury M, Malmgren BA and Winter A (2007) Subregional precipitation climate of the Caribbean and relationships with ENSO and NAO. *Journal of Geophysical Research* 112: D16107. DOI: 10.1029/2006JD007541.

Jury MR (2011) Long-term variability and trends in the Caribbean Sea. *International Journal of Oceanography* 2010: 1–9.

Kameo K, Shearer M, Droxler A et al. (2004) Glacial-interglacial surface water variations in the Caribbean Sea during the last 300 ky based on calcareous nannofossils analysis. *Palaeogeography, Palaeoclimatology, Palaeoecology* 212: 65–76.

Kendall MS, Takata LT, Jensen O et al. (2005) An Ecological Characterization of Salt River Bay National Historical Park and Ecological Preserve, U.S. Virgin Islands. NOAA Technical Memorandum NOS, NCCOS 14: 116 pp. Available at: http://parkscaribbean.net/wp-content/uploads/2013/11/Ecological%20Characterization%20of%20Salt%20River%20Bay%20Park%20(2005).pdf.

Knudsen MF, Seidenkrantz MS, Jacobsen BH et al. (2011) Tracking the Atlantic Multidecadal Oscillation through the last 8000 years. *Nature Communication* 2(178): 1–8.

Koutavas A and Lynch-Stieglitz J (2004) Variability of the marine ITCZ over the eastern Pacific during the last 30,000 years. In: Diaz HF and Bradley RS (eds) *The Hadley Circulation: Past, Present and Future*. Berlin: Springer, pp. 347–369.

Kucera M, Weinelt M, Kiefer T et al. (2005) Reconstruction of sea-surface temperatures from assemblages of planktonic foraminifera: Multi-technique approach based on geographically constrained calibration data sets and its application to glacial Atlantic and Pacific Oceans. *Quaternary Science Reviews* 24(7–9): 951–998.

Kuijpers A and Project Group (2007) Galathea3 – Leg 16 WINMARGIN Project 'West Indies Marine Geoscience Investigations'. Report 2007/44, Geological Survey of Denmark and Greenland, pp. 1–24.

Lea D, Pak DK, Peterson LC et al. (2003) Synchroneity of tropical and high-latitude Atlantic temperatures over the last glacial termination. *Science* 301: 1361–1364.

Levitus S, Burgett R and Boyer TP (1994) *World Ocean Atlas 1994, vol. 3: Salinity*. Silver Spring, MD: NOAA Atlas NESDIS, 111 pp.

López-Otàlvaro GE, Flores JA, Sierro FJ et al. (2009) Late Pleistocene paleoproductivity patterns during the last climatic cycle in the Guyana Basin as revealed by calcareous nannoplankton. *eEarth* 4: 1–13.

Lynch-Stieglitz J, Curry WB and Lund DC (2009) Florida Straits density structure and transport over the last 8000 years. *Paleoceanography* 24: PA3209. DOI: 10.1029/2008PA001717.

McGregor HV, Evans MN, Goosse H et al. (2015) Robust global ocean cooling trend for the preindustrial Common Era. *Nature Geoscience* 8: 671–677.

Malmgren B, Winter A and Chen D (1998) El Nino-Southern Oscillation and North Atlantic Oscillation control of climate of Puerto Rico. *Journal of Climate* 11: 2713–2717.

Malmgren BA, Kucera K, Nyberg J et al. (2001) Comparison of statistical and artificial neural network techniques for estimating past sea surface temperatures from planktonic foraminifer census data. *Paleoceanography* 16(5): 520–530.

Mangini A, Blumbach P, Verdes P et al. (2007) Combined records from a stalagmite from Barbados and from lake sediments in Haiti reveal variable seasonality in the Caribbean between 6.7 and 3 ka BP. *Quaternary Science Reviews* 26: 1332 –1343.

Marshall J, Kushnir Y, Battisti D et al. (2001) North Atlantic Climate variability: Phenomena, impacts and mechanisms. *International Journal of Climatology* 21: 1863–1898.

Martin PA and Lea DW (2002) A simple evaluation of cleaning procedures on fossil benthic foraminiferal Mg/Ca. *Geochemistry, Geophysics, Geosystems* 3: 8401.

Metcalf W (1976) Caribbean-Atlantic water exchange through the Anegada-Jungfern Passage. *Journal of Geophysical Research* 81: 6401–6409.

Morley A, Rosenthal Y and deMenocal P (2014) Ocean-atmosphere climate shift during the mid-to-late Holocene transition. *Earth and Planetary Science Letters* 388: 18–26.

Mulitza S, Dürkoop A, Hale W et al. (1997) Planktonic foraminifera as recorders of past surface-water stratification. *Geology* 25: 335–338.

National Weather Service San Juan, PR Weather Forecast Office (2010) The Local Impacts of ENSO across the Northeastern Caribbean. Available at: http://www.srh.noaa.gov/sju/?n=enso2010 (accessed 2 September 2010).

Nürnberg D (2015) Mg/Ca Paleothermometry – Taking the temperature of past surface oceans. *Encyclopedia of Marine Geosciences*. Epub ahead of print 12 February. DOI: 10.1007/978-94-007-6644-0_98-2.

Nürnberg D, Bijma J and Hemleben C (1996) Assessing the reliability of magnesium in foraminiferal calcite as a proxy for water mass temperatures. *Geochimica et Cosmochimica Acta* 60(5): 803–814.

Nürnberg D, Ziegler M, Karas C et al. (2008) Interacting loop current variability and Mississippi River discharge over the past 400 kyr. *Earth and Planetary Science Letters* 272(1–2): 278–289.

Nyberg J, Malmgren B, Kuijpers A et al. (2002) A centennial-scale variability of tropical North Atlantic surface hydrography during the late-Holocene. *Palaeogeography, Palaeoclimatology, Palaeoecology* 183: 25–41.

O'Connor BM, Fine RA and Olson DB (2005) A global comparison of subtropical underwater formation rates. *Deep-Sea Research* (Part I) 52: 1569–1590.

Olsen J, Anderson NJ and Knudsen MF (2012) Variability of the North Atlantic Oscillation over the past 5,200 years. *Nature Geoscience* 5: 808–812.

Philader SGH, Gu D, Halpern D et al. (1996) Why the ITCZ is mostly north of the equator. *Journal of Climate* 9: 2958–2971.

Poore RZ, Dowsett HJ, Verardo S et al. (2003) Millennial- to century-scale variability in Gulf of Mexico Holocene climate records. *Paleoceanography* 18(2): 1048.

Poore RZ, Quinn TM and Verardo S (2004) Century-scale movement of the Atlantic Intertropical Convergence Zone linked to solar variability. *Geophysical Research Letters* 31: L12214. DOI: 10.1029/2004GL019940.

Regenberg M, Nürnberg D, Schönfeld J et al. (2007) Early diagenetic overprint in Caribbean sediment cores and its effect on the geochemical composition of planktonic foraminifera. *Biogeosciences* 4: 957–973.

Regenberg M, Nürnberg D, Steph S et al. (2006) Assessing the effect of dissolution on planktonic foraminiferal Mg/Ca ratios: Evidence from Caribbean core tops. *Geochemistry, Geophysics, Geosystems* 7: Q07P15.

Regenberg M, Steph S, Nürnberg D et al. (2009) Calibrating Mg/Ca ratios of multiple planktonic foraminiferal species with δ18O-calcification temperatures: Paleothermometry for the upper water column. *Earth and Planetary Science Letters* 278: 324–336.

Reimer PJ and Reimer RW (2001) A marine reservoir correction database and on-line interface. *Radiocarbon* 43: 461–463.

Reimer PJ, Baillie MGL, Bard E et al. (2009) IntCal09 and Marine09 radiocarbon age calibration curves, 0–50,000 years CAL BP. *Radiocarbon* 51: 1111–1150.

Richey JN, Poore RZ, Flower BP et al. (2012) Ecological controls on the shell geochemistry of pink and white *Globigerinoides ruber* in the northern Gulf of Mexico: Implications for paleoceanographic reconstruction. *Marine Micropaleontology* 82–83: 28–37.

Rogers JC (1984) The Association between the North Atlantic Oscillation and the Southern Oscillation in the Northern Hemisphere. *American Meteorological Society* 112: 1999–2015.

Rosenthal Y, Lohmann GP, Lohmann KC et al. (2000) Incorporation and preservation of Mg in Globigerinoides sacculifer: Implications for reconstructing sea surface temperatures and the oxygen isotopic composition of seawater. *Paleoceanography* 15: 135–145.

Ruddimann WF (2003) Orbital insolation, ice volume, and green house gases. *Quaternary Science Reviews* 22: 1597–1629.

Rühlemann C, Mulitza S, Müller PJ et al. (1999) Warming of the tropical Atlantic Ocean and slowdown of thermohaline circulation during the last deglaciation. *Letters to Nature* 402: 511–514.

Schmidt MW, Spero HJ and Lea DW (2004) Links between salinity variation in the Caribbean and North Atlantic. *Nature* 428: 160–163.

Schmidt MW, Vautravers MJ and Spero HJ (2006) Western Caribbean sea surface temperatures during the late Quaternary. *Geochemistry, Geophysics, Geosystems* 7: 2, Q02P10. DOI: 10.1029/2005GC000957.

Schmidt MW, Chang P, Hertzberg JE et al. (2012) Impact of abrupt deglacial climate change on tropical Atlantic subsurface temperatures. *Proceedings of the National Academy of Sciences of the United States of America* 109: 14348–14352.

Schmuker B and Schiebel R (2002) Planktonic foraminifers and hydrography of the eastern and northern Caribbean Sea. *Marine Micropaleontology* 46: 387–403.

Schneider T, Bischoff T and Haug GH (2014) Migrations and dynamics of the intertropical convergence zone. *Nature* 513: 45–53.

Seidenkrantz MS, Roncaglia L, Fischel A et al. (2008) Variable North Atlantic climate seesaw patterns documented by a late-Holocene marine record from Disko Bugt, West Greenland. *Marine Micropaleontology* 68: 66–83.

Stalcup MC and Metcalf WG (1973) Bathymetry of the sills for the Venezuelan and Virgin Islands basins. *Deep-Sea Research* 20: 739–742.

Stalcup MC, Metcalf WG and Johnson R (1975) Deep Caribbean inflow through the Anegada-Jungfern Passage. *Journal of Marine Research* 33: 15–35.

Steph S, Regenberg MTiedemann R, Mulitza S et al. (2009) Stable isotopes of planktonic foraminifera from tropical Atlantic/Caribbean core-tops: Implications for reconstructing upper ocean stratification. *Marine Micropaleontology* 71(1–2): 1–19.

Taylor MA, Enfield DB and Chen AA (2002) Influence of the tropical Atlantic versus tropical Pacific on Caribbean rainfall. *Journal of Geophysical Research* 107: C9: 3127. DOI: 10.1029/2001JC001097.

Telford RJ, Li C and Kucera M (2013) Mismatch between the depth habitat of planktonic foraminifera and the calibration depth of SST transfer functions may bias reconstructions. *Climate of the Past* 9: 859–870.

Toomey MR, Curry WB, Donnelly JP et al. (2013) Reconstruction 7000 years of North Atlantic hurricane variability using deep-sea sediment cores from the western Great Bahama Bank. *Paleoceanography* 28(1): 31–41.

Wang C (2007) Variability of the Caribbean Low-Level Jet and its relations to climate. *Climate Dynamics* 29: 411–422.

World Ocean Atlas (1998) Available at: http://www.geo.uni-bremen.de/geomod/Sonst/Staff/csn/woasample.html.

Worthington LV (1959) The 18°C water in the Sargasso sea. *Deep-Sea Research* 5: 297–305.

Wüst G (1964) *Stratification and Circulation in the Antillean-Caribbean Basins*. New York; London: Columbia University Press, 202 pp.

Zhang R (2007) Anticorrelated multidecadal variations between surface and subsurface tropical North Atlantic. *Geophysical Research Letters* 34: L12713. DOI: 10.1029/2007GL030225.

Ziegler M, Nürnberg D, Karas C et al. (2008) Persistent summer expansion of the Atlantic Warm Pool during the glacial abrupt cold events. *Nature Geoscience Letters* 1: 601–605.